Long-term variation of coronal holes latitudinal distribution

D. A. Maghradze *[1,2], B. B. Chargeishvili†[1], D. R. Japaridze‡[1,2], N. B. Oghrapishvili§[1], and K. B. Chargeishvili¶[1]

[1]Evgeni Kharadze Georgian National Astrophysical Observatory, Mt. Kanobili, Abastumani 0301, Georgia
[2]Centre for Computational Helio Studies, Ilia State University, Cholokashvili Ave. 3/5, Tbilisi 0162, Georgia

Abstract

We study the evolution of the latitudinal distribution of coronal holes using the Solar and Heliospheric Observatory (SOHO)/Extreme ultraviolet Imaging Telescope (EIT) 195 Ådata from 1996 May to 2020 April. To measure the presence of coronal holes at a given latitude, we use the presence factor, which estimates the length of an object along a given parallel, expressed as a percentage of half of the equator length. By semi-automatic processing of the data series, we obtained the 361 ×7346 latitude–time matrix. The corresponding diagram shows the significant difference in evolutionary shapes of a latitudinal distribution of non-polar and polar coronal holes. However, the morphology of the evolutionary picture and the migration route of the geometric centre of activity of the coronal hole in the diagram indicate that non-polar and polar coronal holes have the same driving mechanism. It is believed that the migration of the centre of activity of the coronal hole in the latitude–time diagram is a combination of two opposite migration paths. They intersect at the equator and diverge to opposite poles, where they form the so-called polar coronal holes, then again mo v e to lower latitudes, and this happens cyclically. Determining the opposite migration paths by antiphase sinusoids, their deviation from antiphase determines the detected north–south asymmetry in the activity of the coronal hole.

Keywords: *Solar activity, Solar corona, Solar oscillations.*

1. Introduction

We study the evolution of the latitudinal distribution of coronal holes (CH) activity. Section 2 describes observational data and the methodology we used for our study. Section 3 is dedicated to the results of a study of CH activity over the period from 1996 May to 2020 April and their comparison with activities of sunspots and magnetic field variations. Section 4 discusses the results of the paper.

2. Observational data and methodology of their processing

To reveal the cyclic characteristics of the latitudinal distribution of CHs, it is important to use the data of long-term observations, consisting of at least two cycles of activity. Therefore, instead of higher quality Solar Dynamics Observatory (SDO) data, we use observational data obtained by the Solar and Heliospheric Observatory (SOHO)/Extreme ultraviolet Imaging Telescope (EIT) in a 195 Åfilter. We downloaded a series of daily FITS files from the data base for the period 1995–2020. The main constituent step towards solving scientific problems associated with CHs is their identification and segmentation. Our semi-automated GUI code uses a combination of visual inspection with segmentation by global and local thresholding. The code is modification of the automated processing code described in (Maghradze et al., 2020) (hereafter Paper I). The preprocessing of the data was also carried out using the same procedures as described in Paper I , and we summarize them here. Each file in the series went through the IDL 'EIT PREP.PRO' 'SOLARSOFT' routine, which implies a background-subtracted, degridded, flat-fielded, and degradation-corrected output.

*davit.maghradze.2@iliauni.edu.ge, Corresponding author
†bidzina@aidio.net
‡darejan.japaridze@iliauni.edu.ge
§natela.oghrapishvili@iliauni.edu.ge
¶ketevan.chargeishvili@aidio.net

doi: https://doi.org/10.52526/25792776-23.70.1-27

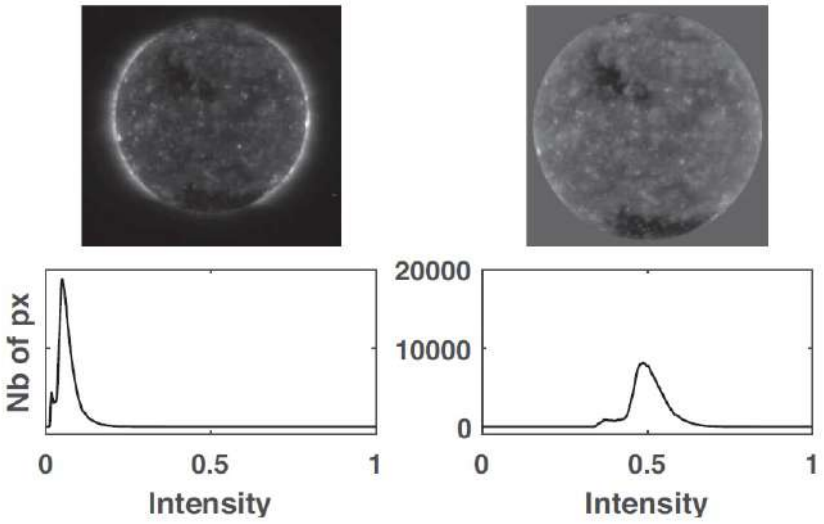

Figure 1. The top left- and right-hand panels display the original image and the image after processing by the modified Bartlett's method. The lower panels are the histograms of the upper images (only the solar disc), respectively.

The intensity threshold required for the segmentation of CHs is not universal and varies not only for different images but also within a single image itself. After converting the image to greyscale with an interval from 0 to 1, to automate the determination of the segmentation intensity threshold, it is necessary to use the features of the image histogram. To do this, we transform the image using a modified Bartlett's (Paper I) method that extracts the root of the power (instead of the Bartlett's square root) so that the average image intensity is 0.5 (see Fig. 1). Because in the identification and segmentation of CHs, the leading role is played by the difference in the intensity of the latter from the environment, it is very important to preliminary remove the artefacts of the change in intensity. The well-known artefact, the limb-brightening effect, caused by the positive altitude gradient of the corona temperature, precludes the application of a single intensity threshold for segmenting an extended object on a disc. Fitting the curves to the centred moving annual average of the empirical intensity distribution profiles from the centre to the limb of the solar disc, they obtained the following radial intensity function:

$$I(i) = a(i)\Big[a^{b(i)\rho} - 1\Big], \tag{1}$$

where $\rho = \dfrac{r}{R_\odot}$ is the dimensionless distance from the solar disc centre normalized on the solar radius $R_\odot$, $a(i)$ and $b(i)$ are parameters calculated by fitting the function (1) to empirical intensity profile of i image.

The right-hand panel of Fig. 2 shows time evolution of $I(i)$ function and one can see a cyclic variation. It is possible to use the pre-calculated coefficients $a(i)$ and $b(i)$ for each image and construct correction image for the limb-brightening removal, but we decided to apply mean curve of I for all images.

The study showed that within the longitudinal limits ± 70 ◦there is no significant deviation between empirical curves of intensity distribution and calculated mean function we use. So the code, using the mean function, creates a correction image (see Fig. 3) to remove the limb-brightening effect. The code then subtracts the corresponding correction image (Fig. 3 (panel c)) from the original, and we get the image without limb brightening. The interactive code interface has the ability to manually adjust the correction image (Fig. 3 (panel b)) for the best result, since the coefficients $a(i)$ and $b(i)$ are obtained by centred moving annual averaging of the intensity profiles, and in some cases the results differ significantly from the real profile of the given image. Another important feature obtained by (Chargeishvili et al., 2019) is that intensity distribution from centre to limb is not polar symmetrical and its isophotes have elliptical shapes with polar elongation. As they show the ratio of major and minor radii is also variable bat mainly it is close to 1.3. The interactive interface of our code has also ability to tune this ratio for better result. After the effect of limb brightening is removed the next step is segmentation of CHs on the disc. To find the

doi: https://doi.org/10.52526/25792776-23.70.1-27

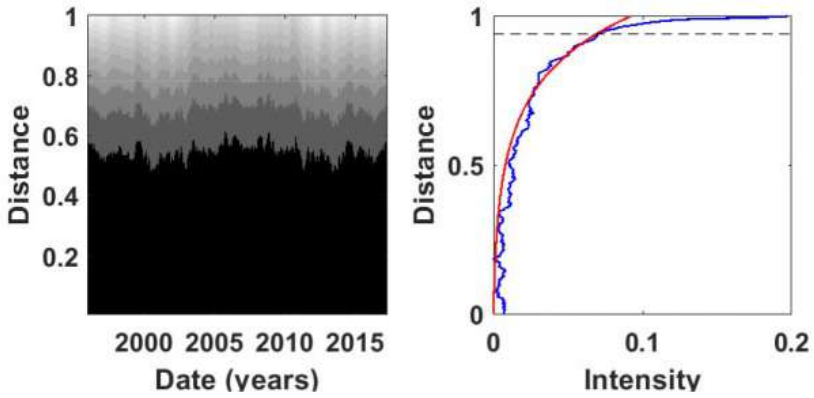

Figure 2. Left-hand panel: evolution of fitted intensity distribution profiles. The right-hand panel is the average of all fitted intensity distribution profiles (red line) and the real intensity distribution profile for a given date (blue line), 70° longitudinal limit (dashed line).

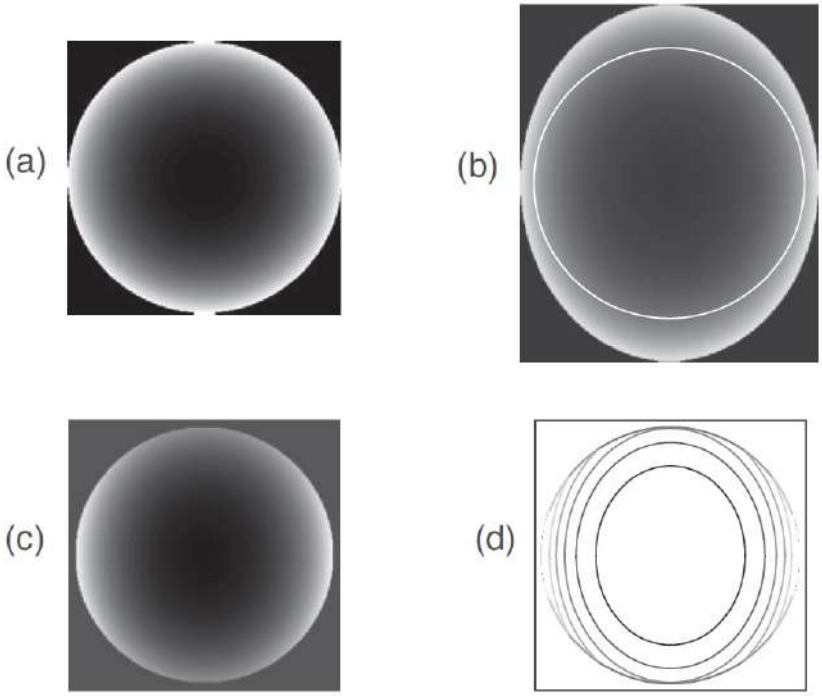

Figure 3. (a) Polar-symmetric correction image obtained by rotating the average of all fitted intensity profiles. (b) Fitting the corrective image to the specified date by elliptical distortion. The white circle is the clipping area for the new correction image. (c) Final correction image. (d) Isophotes of the final correction image.

hump corresponding to the population of dark formations in the resulting histogram, the code smooths the low-intensity wing of the histogram and subtracts the result from the original. On the remaining curve, one gets a concave region, which is easily marked by the code as the intensity threshold (see the top left-hand panel in Fig. 4 and the bottom right-hand panel in Fig. 5) required for segmentation of the CH. Then the code outlines the proposed object. In most cases, this object is indeed a CH, but often the code can outline filaments or coronal dimmings, transition CHs, or even miss any real CHs. In this case, the code has an interactive mode to indicate the region of interest for changing the local intensity threshold, so that the code automatically selects the desired object again. If an object is missegmented, you can undo it separately

from other segmented objects on the disc. In cases where the researcher could not distinguish the probable CH from filaments, the researcher checked in Helioviewer the unipolarity of the suspicious object on the corresponding magnetogram. Also, the code rewind function allows one to check the object in the dynamics of the rotation of the Sun and eliminate confusion with dimmings or transitional CHs.

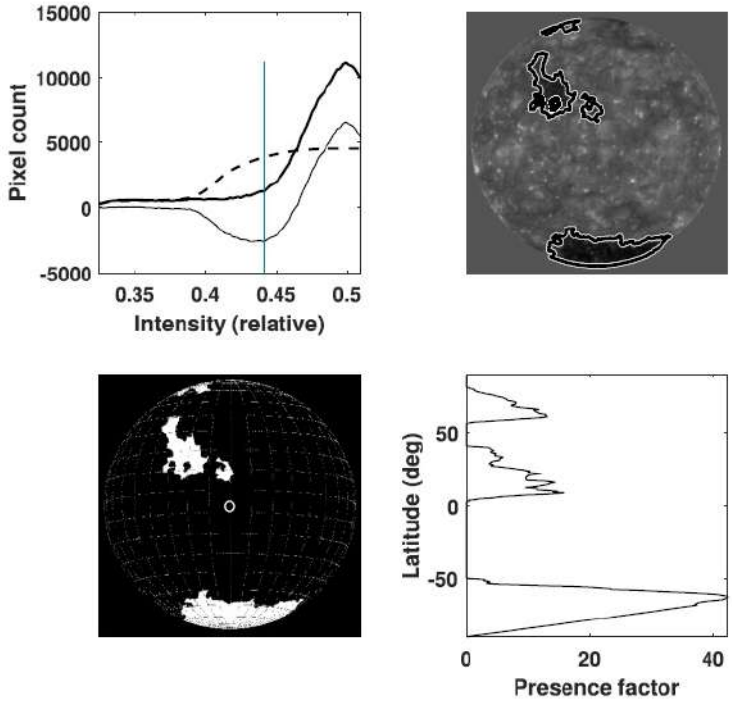

Figure 4. Top left-hand panel: the lower wing of the intensity of the image histogram (bold line), the smoothed histogram (dashed line), the result of their subtraction (normal line), and the threshold (vertical line). Top right-hand panel: segmented CHs on the solar disc. Lower left-hand panel: a binary image of the solar disc and the network of heliospheric coordinates above it. Bottom left-hand panel: distribution of the presence factor (PF) of coronal holes (CHs) at a given date.

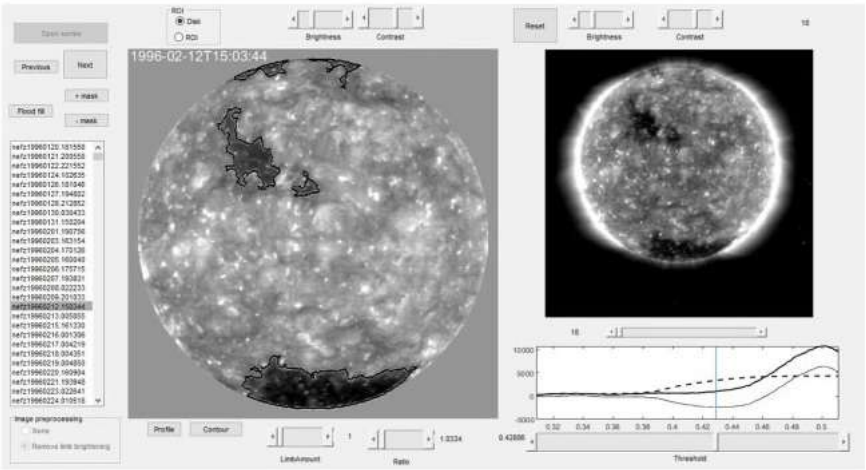

Figure 5. The graphical user interface of the interactive code for CH segmentation and PF latitudinal profile output.

The code, taking the date of observation, Solar-B , solar disc pixel coordinates, and solar disc pixel radius from the FITS file header, operates in heliographic coordinates. The code scans the segmented binary image

doi: https://doi.org/10.52526/25792776-23.70.1-27

of the solar disc within the ranges ±90 latitudes and ±80 longitudes both with spans of 0°.5 and gets data from 361321 points of a disc. Finally, profiles of PFs of each image from the data series are compiled in a latitudinal data matrix.

Since SOHO /EIT observational data have gaps in everyday observations, and also not all images obtained are suitable for processing, the final data are not sampled uniformly. To correctly go through the necessary procedures (say, annual moving averaging) or to compare the CH activity with the activity of the polar magnetic field or the number of spots, we interpolated all variables in the same time domain with uniform sampling.

3. CH activity and relation with sunspots and magnetic fields

We begin the description of our results with the most obvious diagram showing the time evolution of the CH activity latitudinal distribution during more than two solar activity cycles (Fig. 6).

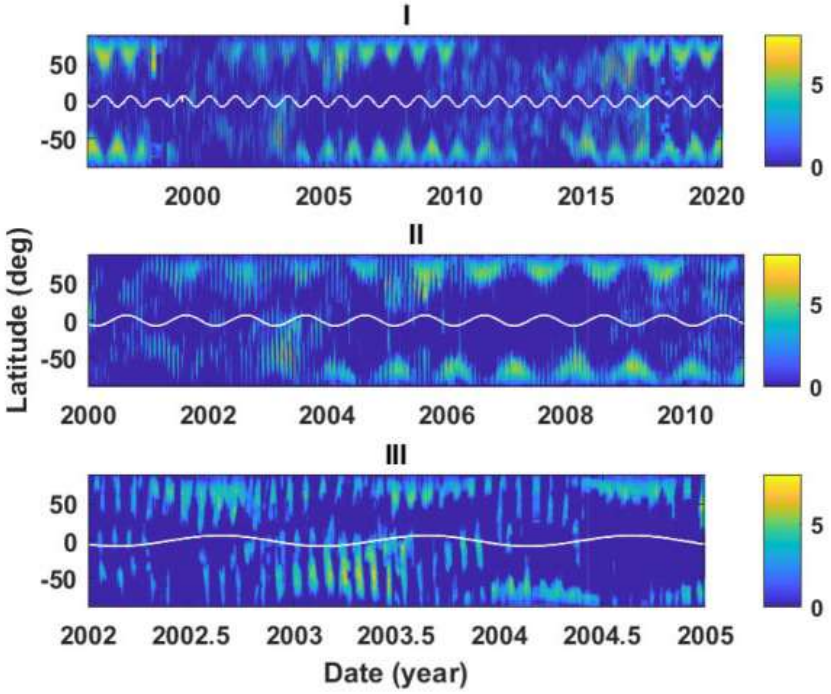

Figure 6. Latitude–time distribution of CHs (from 1996 May to 2020 April). The horizontal axes show time in years, and the vertical axes show latitude. The solid white lines show the change in the heliographic latitude of the central point of the solar disc. The first panel shows the latitudinal distribution of the PF for the entire study period. The second and third panels show the same as the first, but for shorter periods. For better visualization, the square root of the PF values is used.

In general, an approximately 11-yr recurrence of features is typical for all latitudinal zones, but the difference in activity at polar and middle latitudes is obvious. In the polar regions mostly and with a lesser intensity in the mid-zone, along with the 11-yr cycle of solar activity, an annual periodic variation is evident. We also disco v er a shorter, quasi-monthly period in the middle part of the diagram along with north–south asymmetry seen in polar regions. The annual oscillatory structure of the evolution of CH activity closely correlates with the annual variation of the solar B_0 angle, heliographic latitude of the central point of the solar disc. The simplest explanation that comes to mind is that the fluctuation should be observational only and should be caused by the geometric effects of the B_0 variation. CH is not a plain dark place on the surface of the corona. It is the place where the radial open magnetic field arising from the Sun to our sight is confined. The CH is surrounded by closed magnetic structures holding denser and brighter plasma.

We divide the Sun's surface into three zones: north polar, south polar, and mid-latitudes. We consider it useless to divide middle latitudes into northern and southern zones due to the large size of some CHs (they often cover both sides of the equator). We use the following notation: NPZ and SPZ for the north and south polar zones, respectively; MZ for the middle zone; and TZ for the total disc. For ease of comparison

doi: https://doi.org/10.52526/25792776-23.70.1-27

of results in different hemispheres and comparison with the results of the magnetic field and the number of sunspots, we evaluate the CH activity by the value of PF on a 10-point system. We presume that the maximum value of the averaged PF for the entire Sun is equal to 10 conventional magnitudes.

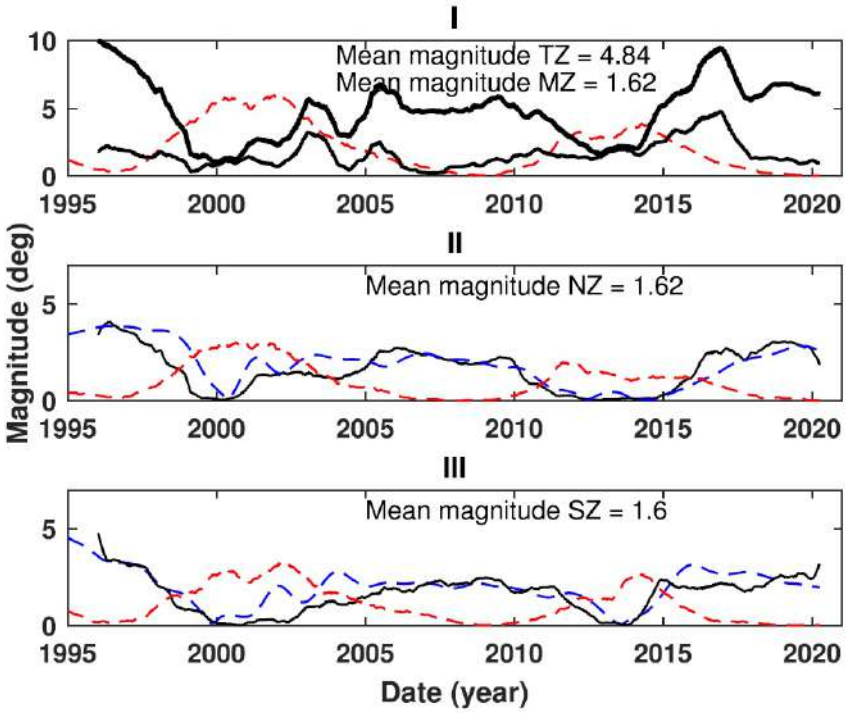

Figure 7. Activity curves. (I) Centred annual moving average of CH activity for the entire disc (black bold solid line), centred annual moving average of CH activity in the middle zone (black solid line), and centred annual moving average of sunspot numbers (red dashed line). (II) Centred annual moving average of CH activity in the north polar zone (black solid line) and averaged north polar magnetic field (blue dashed line). (III) Centred annual moving average of CH activity in the south polar zone (black solid line) and averaged south polar magnetic field (blue dashed line). The red dashed lines represent the sunspot numbers in both hemispheres (panel I) in the Northern and Southern hemispheres (panels II and III, respectively.

Fig. 7 shows different patterns of CH activity in three zones. In general, the CH activity with an average magnitude of about 5 is in antiphase with the sunspot number activity (Fig. 7 (panel I)). Whereas, the middle zone having the average magnitude of activity of about 1.62 is almost in phase with the activity of sunspots with some noticeable delay. In both polar zones (Fig. 7 (panels II and III)), CH activities are in antiphase with sunspot activity and show good coincidence with polar magnetic field cyclic variations. The evolution patterns of CH activities in different polar zones are similar to each other and have similar mean values of activity magnitudes (1.62 and 1.60 for northern and southern polar zones, respectively). Fig. 7 (panel II) and (panel III) show a close correlation between the activity patterns of polar magnetic fields and polar CHs, with correlation coefficients of 0.82 and 0.79 for the Northern and Southern hemispheres, respectively. We found it more convenient to compare the data of polar CHs and polar magnetic fields with the sunspot data flipped up-down (Fig. 8). The correlation between polar magnetic fields and the flipped number of sunspots has very high significance ($p = 0$) with coefficients of 0.39 and 0.46 for the Northern and Southern hemispheres, respectively. We can only compare the activity of CHs and the number of sunspots in the last two cycles. Since variations in the activity patterns of polar CHs and magnetic fields are in such close correlation (which is quite natural), we can compare the activities of magnetic fields and sunspots. The results can be generalized to CHs. So, for example, we see that the durations of minima of CH activities are different in different hemispheres. It fits well with the durations of maxima of the numbers of sunspots in these hemispheres. Comparing the curves of the magnetic field and sunspots, we can say that, in general, the duration of the minima of polar CHs and magnetic fields in each hemisphere correlates well with that of the maximums of sunspots in these hemispheres. We know that sunspots perform their activity in regions of low latitudes, completely different from the region of polar magnetic fields and polar CHs. Such a close correlation between them leads us to the idea that the polar magnetic field (and hence the polar CHs) and

doi: https://doi.org/10.52526/25792776-23.70.1-27

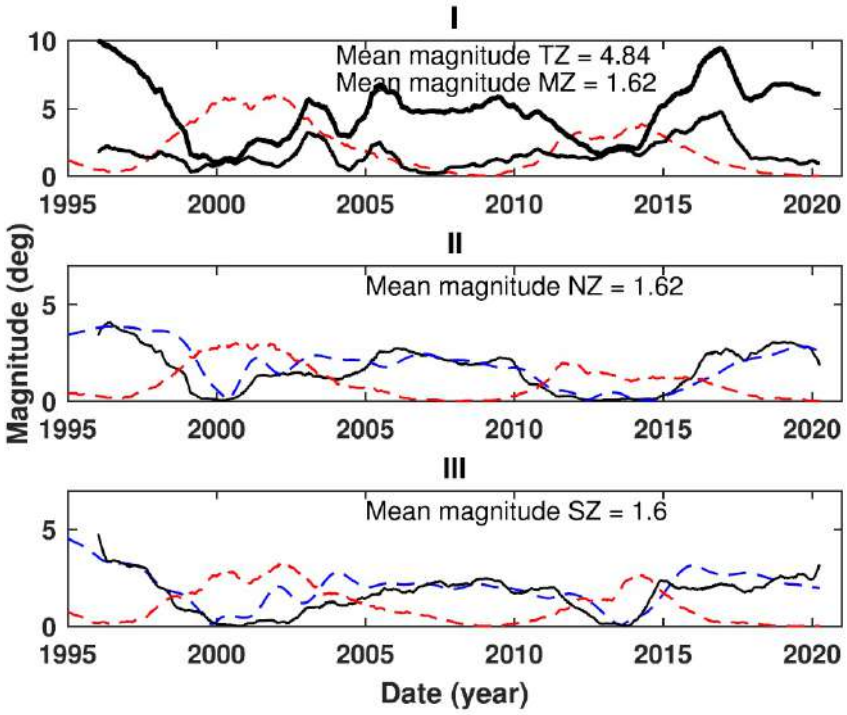

Figure 8. Correlation of the activity of polar CHs (black line) with the activity of the polar magnetic flux (red line) and a hemispheric sunspot numbers (blue line) for the Northern (panel I) and Southern (panel II) hemispheres.

sunspots have a common driving mechanism. Along with sunspots, non-polar CHs should play an important role in the transfer of the magnetic field. But, as can be seen from Fig. 7, the shape of the activity curve of non-polar CHs does not correlate as well with the shapes of the polar curves as the shapes of the activity curves of sunspot numbers in the hemispheres. This may be due to the fact that we cannot assign non-polar CHs to different hemispheres. Looking at Fig. 7 the non-polar zone leaves an impression that it is the exchange area of large-scale open magnetic fluxes (CHs) between polar zones.

To better understand details of latitudinal migration of CH activity, we calculated geometrical centres of PF for all CHs and separate zones. Separate zonal migrations of activity centroids did not reveal any interesting features. The reason we discuss below. As for the migration of PF centroids for the whole disc CHs, we present it over the time latitude diagram of PFs in Fig. 9.

Fig. 9 shows that, despite some deviations during the active phase of cycle 23, the centre of activity is in the Northern hemisphere, and in the phase of minimum sunspot activity moves to the Southern hemisphere and remains there during cycle 24.

4. Conclusions

This study deals with the variation of the latitudinal distribution of CHs. We used SOHO /EIT 195Å daily data from 1996 May to 2020 April. To correctly measure the levels of CH activity at any latitude, we use the so-called CH PF, which estimates the length of an object along a given parallel, expressed as a percentage of half the equator length. After semi-automatic processing of 7346 FITS files, we obtained a 3617346 data matrix for the CH PF values. The resulting diagram (Fig. 6) demonstrates a clear structuring of the time–latitude distribution of PF. The character of structuring differs in the polar and middle zones. According to the local entropy distribution of PF, we divided the Sun into three zones of activity. Zone delimiters come at ±53° of latitude. All three zones show oscillatory-type evolution of the CH activity and oscillation with annual periods is dominant. The annual oscillations are in antiphase with the variations of Solar-B. Their amplitudes are comparable at the equator, and the amplitude of the oscillatory pattern grows to wards the higher latitudes.

Annual periodicity is dominant in all zones. Another prominent period is about the synodic period of

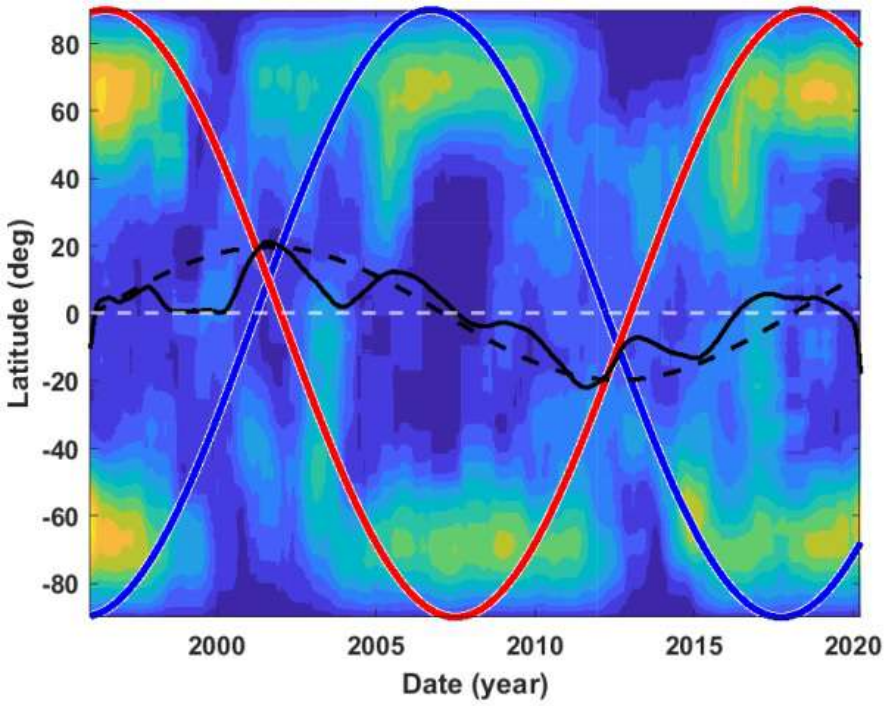

Figure 9. Latitudinal migration of CH activity centroids plotted on the time–latitude diagram of PFs. The black curve is the empirical path of the PF centroids. Red and blue lines indicate simulated migration paths of CHs with oppositely directed magnetic fluxes. The black dashed curve is a superposition of the red and blue curves.

solar rotation. It is reflected in the diagram (Fig. 6) in the form of thin vertical fibres and should be caused by a long lifetime of CHs (several months) along with the hiding of open-structured magnetic features by closed ones.

It should be mentioned that the fact that the SOHO data are obtained from the ecliptic plane gives a significant uncertainty in obtaining the PFs near the pole regions due to the spherical geometry and the projection effect. Moreover, when determining the geometric centre of the PFs near the poles, we cannot take into account the possible existence of CHs on the other side of the disc, and in this case, we obtain centres shifted to lower latitudes.

A key result of this work is that large-scale fluxes of a unipolar magnetic field, the visual manifestation of which are CHs, do not belong to separate zones or even separate hemispheres on their cyclic evolutionary path. On the contrary, we found that the migration of the CH activity centre must be a superposition of two opposite migration paths, as shown in Fig. 9. These migration routes intersect at the equator and diverge to opposite poles, where they form the so-called polar CHs, then again move to non-polar zones, and this repeats cyclically. We considered the opposite migration paths to be governed by antiphase sinusoids. A small deviation from antiphase (0.07π) determines the detected north–south asymmetry in the activity of the CH. The close correlation between sunspot activity and CHs indicates that the generation of large-scale and compact magnetic fluxes is driven by a common mechanism. The results are important for elucidating the details of the mechanism of the magnetic dynamo. In the future, we intend to detail the picture of the evolutionary CH migration by identifying the polarity of the already identified CHs and thereby determining the polarity of the migration paths.

References

Chargeishvili B. B., Maghradze D. A., Japaridze D. R., et al. 2019, Adv. Space Res., 64, 491–503

Maghradze D. A., Chargeishvili B. B., Japaridze D. R., et al. 2020, Adv. Space Res., 65, 1321 (Paper I)